Chapter-5

Catalytic behavior of $Pr_{1-x}Ba_{1+x}Co_2O_{6-\delta}$ in alkaline medium

Publication: ***Ajay S. Bangwal, Manisha Chauhan and Prabhakar singh***, *Int. J. Hydrogen energy. DOI : 10.1016/j.ijhydene.2022.02.002*

CHAPTER 5: Catalytic behavior of $Pr_{1-x}Ba_{1+x}Co_2O_{6-\delta}$ in alkaline medium

5.1 Introduction

The necessity of renewable energy sources may be confronted with advanced electrochemical energy storage devices. These devices play vital roles in electrified transportation, modern electronics, and clean energy[166],[167]. Many electrochemical processes are the defining factors for the conversion process in electrochemical devices. The layout of the electrochemical devices may be complex, but the basic concepts are relatively straightforward. These systems are a two-electrode system where anode involves OER, whereas the cathode part involves ORR or HER[170]. In electrochemical energy conversion devices and storage technologies such as fuel cells or rechargeable batteries, ORR governs the energy-transfer efficiency whereas HER is the cathodic reaction of electrochemical water splitting, and OER is the complementary anodic half-reaction. Driving the HER with renewable energy sources can lead us to a sustainable hydrogen fuel source used in combustion engines as a zero-emission fuel cell. Out of these electrochemical reactions, ORR has a special place in the process of electrocatalysis. This process is a four electron-proton reaction complemented by the production of electrical potential. However, it has a kinetically lethargic step. In recent years, substantial research has been performed in this field[171]–[174]. To achieve the desired current density, a high rate of overpotential is required, that can be fulfilled by a highly active OER catalyst.

A noble metal-based catalyst such as RuO_2, IrO_2, Pt, and its alloys have been found to work as a significant ORR or OER catalyst for a long time, but their high cost constraints

their large-scale applications[175]. This shifts the interest of the scientific community towards the development of non-precious OER catalysts. Many research works were also focused on catalysts (non-noble) such as Fe and Co- macrocycles due to their remarkable selectivity and reasonable activity towards ORR. However, their low stability in an acidic medium is a foremost shortcoming[176]–[178].

Perovskite oxides (ABO_3) have been noticed to receive substantial attention in past decades in the energy-related field, such as critical materials for high-temperature energy devices (solid oxide fuel cells)[179], materials as an oxygen-transporting membrane for the application of oxy-fuel combustion[180], and as material for solar cells for solar energy harvesting [181]. In recent years, perovskite oxides have also emerged as a promising class of electrocatalysts (non-precious) OER and ORR in an alkaline medium with their excellent oxygen mobility and defective structure.[182][183][184]. Fe doped $SrTi_{0.1}Co_{0.9}O_{3-\delta}$ illustrates good OER activity and stability in alkaline media[185]. $La_{0.4}Sr_{0.6}Co_{0.7}Fe_{0.2}Nb_{0.1}O_{3-\delta}$ offered superior performance as a bifunctional oxygen electrocatalyst[186]. Calcium substituted lanthanum ferrites ($La_{1-x}Ca_xFeO_{3-\delta}$)[187]. $Ba_{0.5}Sr_{0.5}Co_{0.8}Fe_{0.2}O_{3-}\delta$[188], $Sr_{0.95}Ag_{0.05}Nb_{0.1}Co_{0.9}O_{3-\delta}$[189], $La_{0.5}Sr_{0.5}CoO_{2.91}$[190] are such kind of perovskites which extend a new facet of electrocatalyst. Compared to traditional perovskites, double perovskites $AA'B_2O_{5+\delta}$ offered much faster ORR. This is due to their higher surface-exchange coefficient and higher ion diffusion rate [191]. The family of $LnBaCo_2O_{6-\delta}$(Ln=Pr, Sm, Gd, and Ho) has been reported as a highly active catalyst for alkaline solutions[89]. Among the various $LnBaCo_2O_{6-\delta s}$, $PrBaCo_2O_{6-\delta}$ exhibits superior OER and HER activities[89], [192]. Although, double perovskites are studied widely as a catalyst for OER and HER rather than ORR.

The OER activity of perovskites and double perovskites depends on the amount and nature of the A-site and B-site elements.[193][194] . Tailoring the composition of A-site as well as B-site can enhance the electrocatalytic activity in double perovskites. In recent years, several research papers have been published with tailoring the perovskite oxide composition like Jinsuntivich et al. reported the intrinsic OER activity in $Ba_{0.5}Sr_{0.5}Co_{0.8}Fe_{0.2}O_{3-\delta}$(BSCF)[195]. Later, Xu et al. devolved another electrocatalyst via A- site Pr doped BSCF, $Pr_{0.5}(Ba_{0.5}Sr_{0.5})_{0.5}Co_{0.8}Fe_{0.2}O_{3-\delta}$ along with the tuning of its electronic structure.[196] similarly, Zhao et al. observed that the electrochemical activity of $PrBaCo_2O_{6-\delta}$ can be enhanced by co-doping of strontium and iron [197]. However, the effect of substitution on ORR or OER activities in double perovskites is least studied and yet to be investigated thoroughly.

In previous chapter, the compositional effect of ORR in Pr doped $Pr_{1+x}Ba_{1-x}Co_2O_{6-\delta}$ was studied and observed that it enhances ORR's catalytic activity with more hydrogen gas production. To understand the impact of A-site substitution, in this chapter, we synthesized and reported a novel series of catalyst $Pr_{1-x}Ba_{1+x}Co_2O_{6-\delta}$ (x = 0.05, 0.10, 0.15, and 0.20) by changing the A-site stoichiometry with Ba substitution using the conventional solid-state route. The structural and microstructural studies of the synthesized electrode samples are studied. Addistionally, in the present investigation, their electrochemical activities towards OER and ORR in alkaline solution are studied using cyclic voltammetry.

5.2 Experimental Procedure

5.2.1 Chemicals, Synthesis and measurements

A series of double perovskite $Pr_{1-x}Ba_{1+x}Co_2O_{6-\delta}$, (x = 0.05, 0.10, 0.15 and 0.20) were synthesized using the conventional solid-state reaction route. Pr_6O_{11} (99.5 %), $BaCO_3$ (99 %), and Co_3O_4 (99.7 %) procured from Alfa-Aesar were used as raw materials. Stoichiometric amounts of these materials were weighed according to the desired compositions of the samples. The mixtures were ground thoroughly and then wet ground for 5 to 6 h with agate mortar in the acetone as a mixing medium. The samples were further calcined at 1000 ^oC and consequently sintered at 1050 °C for 10 h.[198]. The samples were ground before sintering and pelletized using a hydraulic press and applying a pressure of 4-5 kg/m^2. The heating rate was maintained at 5 ^oC / min. for both the calcination as well sintering processes. TGA and DSC measurements (Mettler Toledo, Germany) were performed at a temperature range from 30 to 1000 °C at a heating rate of 5 °C /min. in a nitrogen atmosphere. The phase identification of the sintered sample was performed employing X-ray diffraction analysis using RIGAKU MINIFLEX600 system with Cu-Kα radiation (λ ~1.5406 Å) in the 2θ range from 20° to 70° with a step size 0.01° at a scan rate of 5°/min. Surface morphology was analyzed with EVO-Scanning Electron Microscope MA15/18. Average size distribution was determined with Zetasizer Pro (Malvern instrument Ltd.). The electrochemical measurements were performed using a Keithley 2450 source meter.

5.2.2 Electrode preparation and electrochemical measurements

To perform the cyclic voltammetry and other electrochemical measurements, three electrodes set up was used. Ag/AgCl electrode kept in 1 M KCl solution was used as a reference electrode, and Pt wire was used as a counter electrode. The pallet of 10-12 mm diameter and thickness of around 0.3-0.5 mm was prepared and attached with copper wire to convert the $Pr_{(1-x)}$ $Ba_{(1+x)}Co_2O_{6-\delta}$ into working electrodes. The concentration of electrolyte solution used for this setup was 1M KOH solution. The potential measured in the electrolyte solution was a reference to the Ag/AgCl electrode. All the measurements were done after the stabilization of open-circuit voltage V_{OC}. Cyclic Voltammetry (CV) was performed with a scan rate of 20 to 200 mV/s. The potential was varied between -1.5 to +1.5 (Ag/AgCl) (and vice versa). Specific capacitance was recorded in the range of scan rate from 10 mV s^{-1} to 200 mV/s. Electrochemical performance for HER or ORR was analyzed using the CV data recorded at the scan rate of 20 to 250 mV/s. The long-term stability of the electrodes was calculated using Chronopotentiometry with a constant current density of 10 mA/Cm^2 for 10^4 seconds and with a contact voltage of +1 Volt, respectively.

5.3 Results and Discussion

5.3.1 Thermogravimetry analysis

The calcined powders' thermal behavior was studied by thermogravimetric analysis in an N_2 atmosphere from room temperature to 1000 °C and shown in figure 5.1. The first decomposition state occurs at ~210 °C in all the samples, which can be assigned to releasing the adsorbed water from the sample surface[199]. All the samples began to lose their weight at ~250 °C and gradually decreased with the higher temperature. These phenomena can be

related to the thermal-driven release of lattice oxygen, which was previously reported for the other cobalt-based perovskite oxides[94]. The weight loss can be divided into three steps, as shown in the figure for different processes. From the TGA graph, the total weight loss is 1.81 % for x = 0.05, 2.31% for x = 0.10, 1.83 % for x = 0.15, and 2.47 % for x = 0.20. To calculate the decomposition temperature, the derivative of mass loss is also plotted against the temperature in figure 5.1. There is a peak in the derivative of weight loss for all the samples in the range of 200 °C-230 °C, indicating a mass gain. This mass gain in the N_2 atmosphere is due to stoichiometry (change in δ)[200]. A deep hump has occurred around 985 °C in all the samples indicating the phase formation.

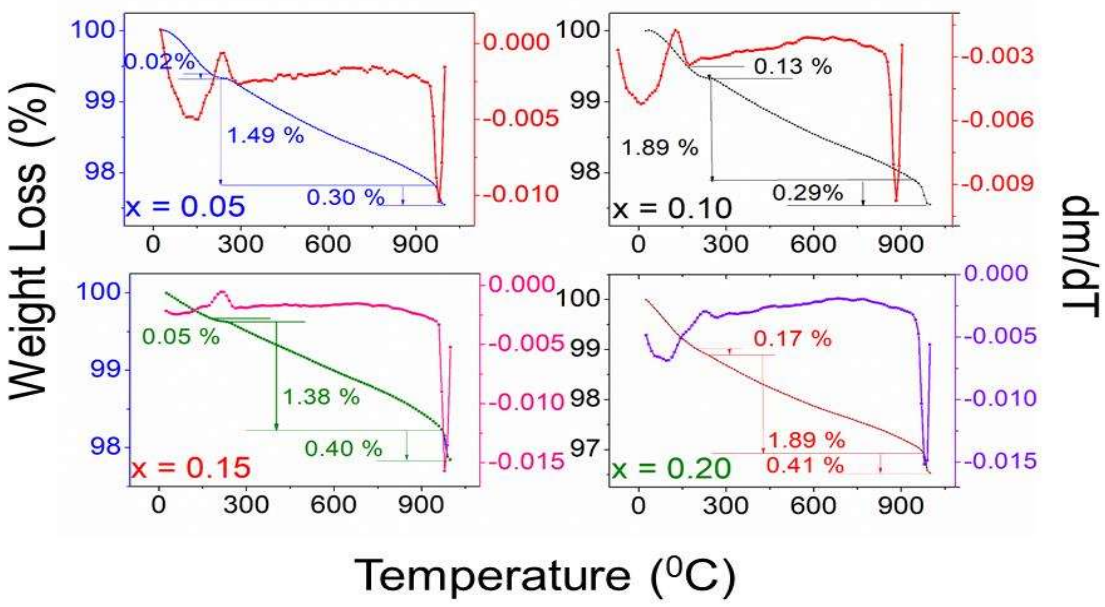

Figure 5.1: TGA curve of the $Pr_{1-x}Ba_{1+x}Co_2O_{6-s}$ samples in N_2 atmosphere

5.3.2 Structural and microstructural studies

XRD pattern of sintered samples, as shown in figure 5.2(a), was analyzed to identify the crystal structure. All samples have the orthorhombic phase similar to $PrBaCo_2O_{6-\delta}$. All significant peaks are indexed. As the concentration of Ba increases, the major peak is shifting

towards a lower angle up to x = 0.90, which may be because of higher ionic radii of Ba^{2+} (1.35 Å) compared to that of the Pr^{3+}(0.99 Å). Close view of XRD in 2θ range 30° - 34° is showing an additional peak at 31.36° (103) in x = 0.85, which can be assigned with $BaCoO_{0.23}$ (JCPDS- 47-0211). Phase of $PrCoO_3$ is also observed in x = 0.05 and x = 0.15. Two-phase Rietveld refinement was performed to identify phase symmetry and lattice parameters [figure 5.2(c)]. All the samples, except x= 0.15, show good refinement from the Orthorhombic phase and Pmmm symmetry. Since the pure phase formation in x=0.15 is questionable, further study was performed only in three samples (x=0.05, 0.10 and 0.20) with reference to x= 0.0. All the parameters obtained from Rietveld refinement are listed in table 5.1.

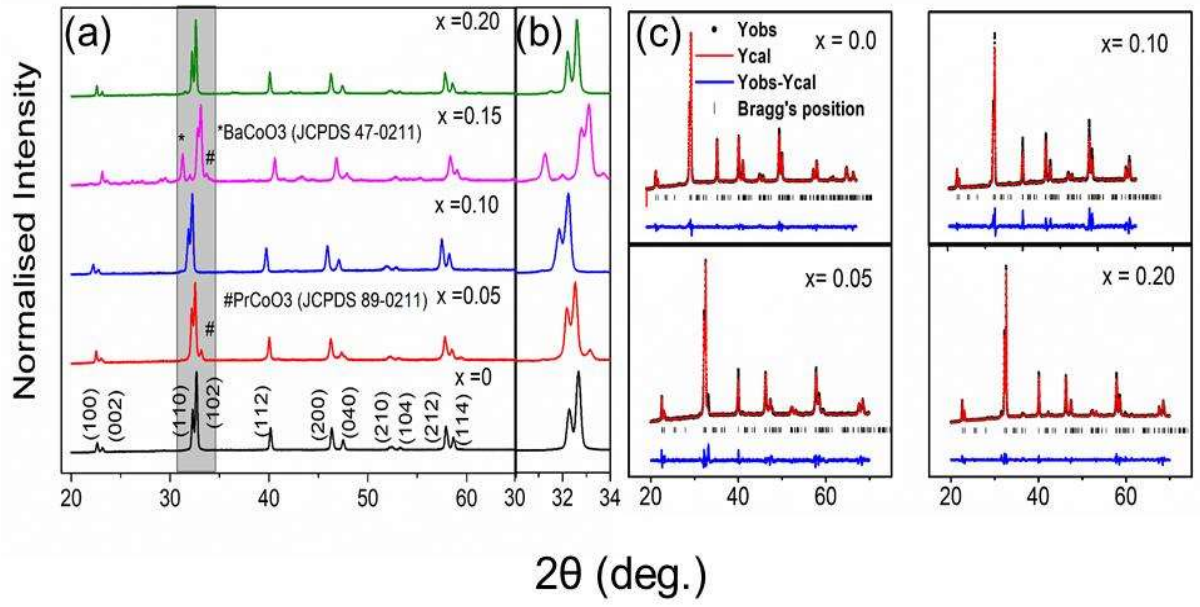

Figure 5.3: X-ray diffractograms of the compositions $Pr_{1-x}Ba_{1+x}Co_2O_6$ $_1$(b) Magnified XRD graph (c) Rietveld refined XRD graph of $Pr_{1-x}Ba_{1+x}Co_2O_{6-\delta}$ (x=0.0,0.5,0.10 and 0.20)

Sample	x=0.05	x=0.10	x=0.20
Symmetry	Pmmm	Pmmm	Pmmm
a(Å)	3.9263	3.9291	3.9227
b(Å)	7.8367	7.8687	7.8521
c(Å)	7.6987	7.6902	7.6174
Density (g/cm3)	7.52	7.521	7.611
Volume((Å3)	237.7022	237.7555	236.2877
χ^2	4.85	6.41	5.36

Table 5.1: Rietveld refinement parameter for $Pr_{1+x}Ba_{1-x}Co_2O_{6-\delta}$ (x=0.05,0.10 and 0.20)

5.3.3 Microstructural studies

Figure 5.3 represents the SEM micrographs of all the sintered samples. It is interesting to observe that the morphology of all the samples is different. Grain formation in x=0.10 and x =0.15 is rectangular in size, having a layered structure. While in the case of x = 0.05 and x=0.20, grains are roughly circular in size. One more interesting feature that can be observed is that these samples are thoroughly porous. Porosity is a vital characteristic of the cathode materials for solid oxide fuel cells as they have to transfer oxygen across gain and grain boundaries. EDX microanalysis of the sample is performed for the element compositions and shown in figure 5.4, revealing that only the components Pr, Ba, Co, and O are identified on the surface of the sample with no impurities. Along with the atomic % of the element determined experimentally (through EDX), the atomic % computed stoichiometrically is also presented. The experimental EDX confirms the elemental content as per the stoichiometric calculations, within an error of 10%. All of the samples, including x = 0 ($PrBaCo_2O_{6-\delta}$) have

become oxygen deficient. This happens because oxygen is volatile enough due to its low band dissociation energy[201].

The average particle size was determined by the DLS technique. The suitable parameters were chosen for each electrocatalyst. The average particle size was obtained as 504.3 nm for x=0, 540.5 nm for x=0.05, 423.1 nm for x=0.10 and 563.4 nm for x =0.20. Since the electrocatalysts were synthesized through a solid-state route, the average particle size is higher. However, this particle size is acceptable for a catalyst activity[202]. The size distribution curve of all the samples is shown in figure 5.5.

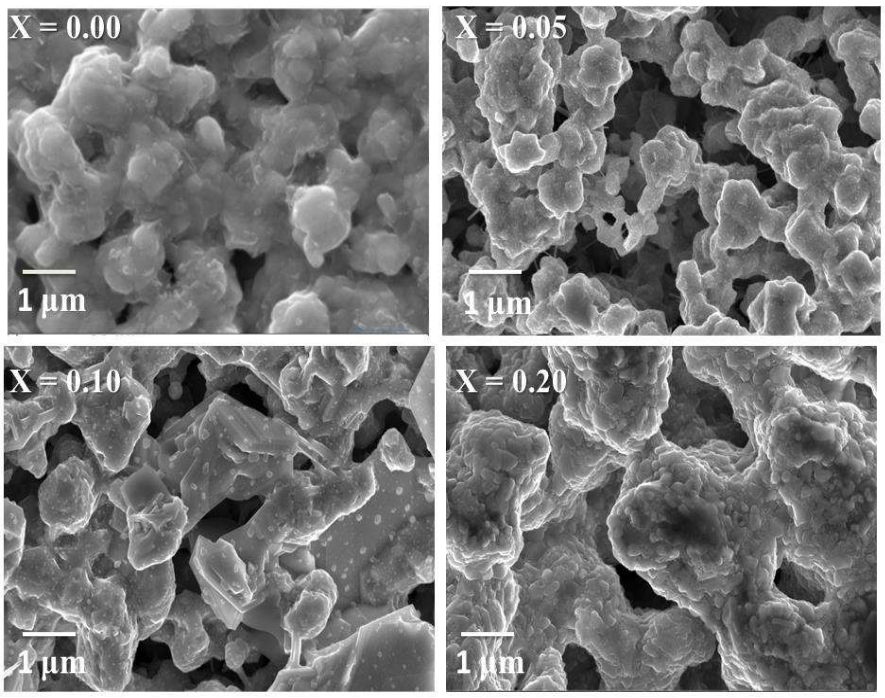

Figure 5.3: SEM images of $Pr_{1-x}Ba_{1+x}Co_2O_6$ (x= 0.0, 0.05, 0.15 and 0.20)

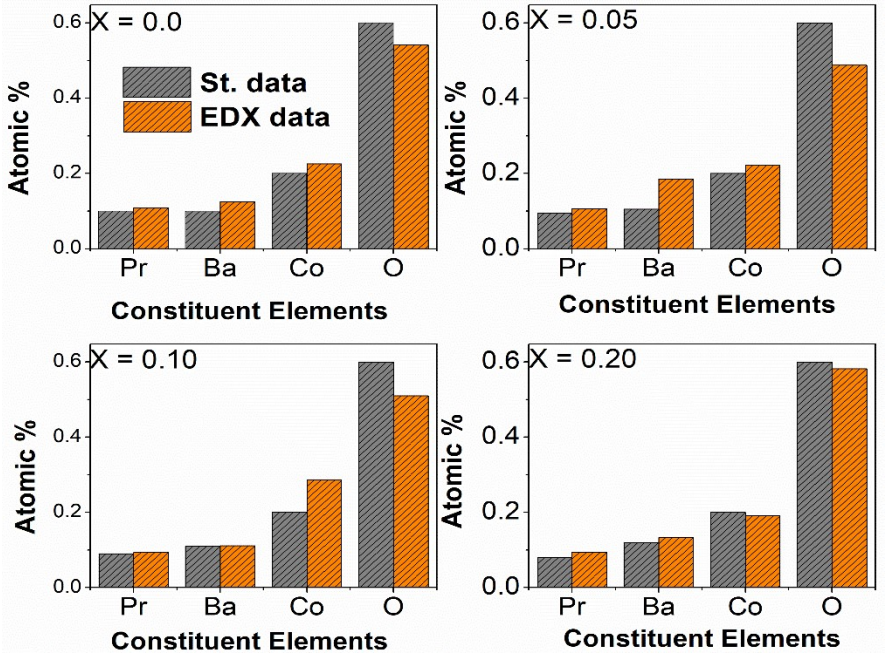

Figure 5.4: EDX images of $Pr_{1-x}Ba_{1+x}Co_2O_6$ (x= 0.0, 0.05, 0.15 and 0.20)

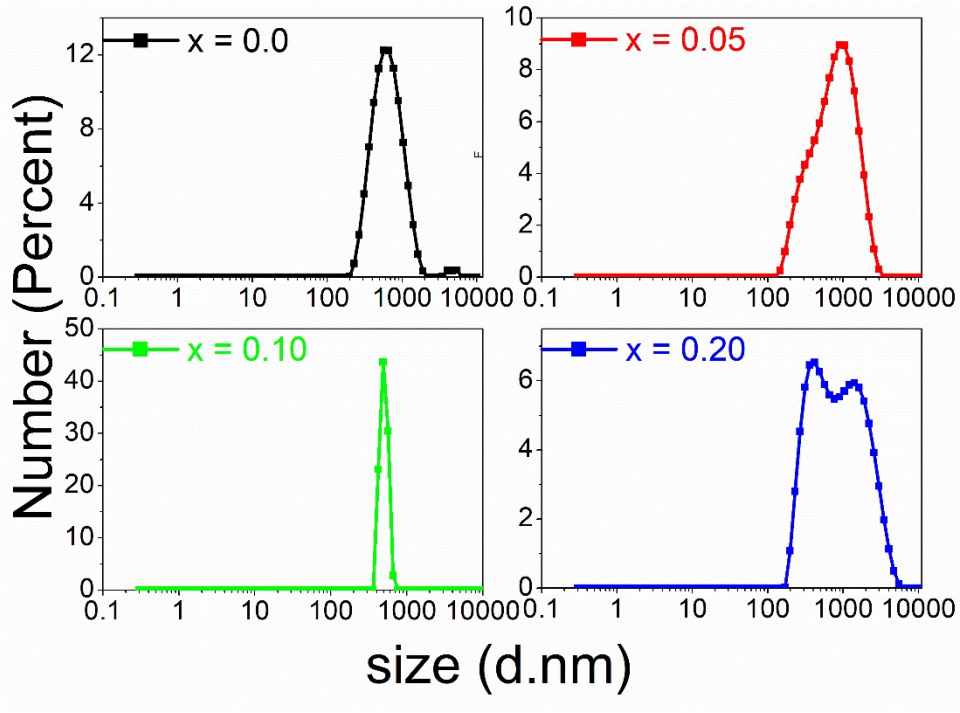

Figure 5.5: Size distribution of the $Pr_{1-x}Ba_{1+x}Co_2O_{6-\delta}$ by number. Dispersant is ethanol.

5.3.4 Electrochemical catalytic activity

The catalytic activity of all the samples were investigated using cyclic voltammetry (CV) in a three-electrode system in a potential range (-1.5 to 1.5 V). In cyclic voltammetry, a curve has been plotted for all the synthesized samples at a scan rate of 50 mV/S to understand Oxygen reduction reaction. Figure 5.6 shows the CV curve for all the electrode samples at the scan rate of 50 mV/S in 1 M Na_2SO_4 electrolyte solution. The open-circuit voltage V_{OC} was stable in all the samples. The value of V_{OC} is 0.33V, 0.49V, and 0.27 V for x = 0.05, x =0.10 and x=0.20, respectively. A strong redox peak was observed in x= 0.05 in the cathodic region (IIIrd quadrant) at 0.78 volts. This peak in the cathodic scan process is due to the oxidation state of B site cation Cobalt, indicating its reduction from Co^{3+}/Co^{4+} to Co^{2+}/Co^{3+} [203]. The below equation can describe the redox process of Cobalt in KOH electrolyte:

$$(OH)_2 + OH^- \leftrightarrow CoOOH + H_2O + e^- \qquad (5.1)$$

$$CoOOH + OH^- \leftrightarrow CoO_2 + H_2O + e^- \qquad (5.2)$$

In the parent sample, x= 0.0, a peak was observed in both the cathodic and anodic regions; however, the value of cathodic current is much higher in the case of x=0.5 than the x =0.0. However, the shape of the CV curve in x = 0.10 is quasi rectangular shape with a partial redox peak in the anodic region (Ist quadrant). This symmetry suggests a diffusion-limited faradic mechanism, electric double layer capacitive mechanism, and surface redox reactions (pseudocapacitive)[204]. The cathodic and anodic current position areas in x=0.0, 0.05, and x=0.10 are overlapped during multiple scans, indicating good cyclic stability and electrochemical reversibility. The current density for the various scan rates is demonstrated in figure 5.7. The peak current density increases as we increase the scan rate. This

phenomenon represents rapid ionic and electronic transport rates and occurs due to the reduction in the size of the diffusion layer.[205].

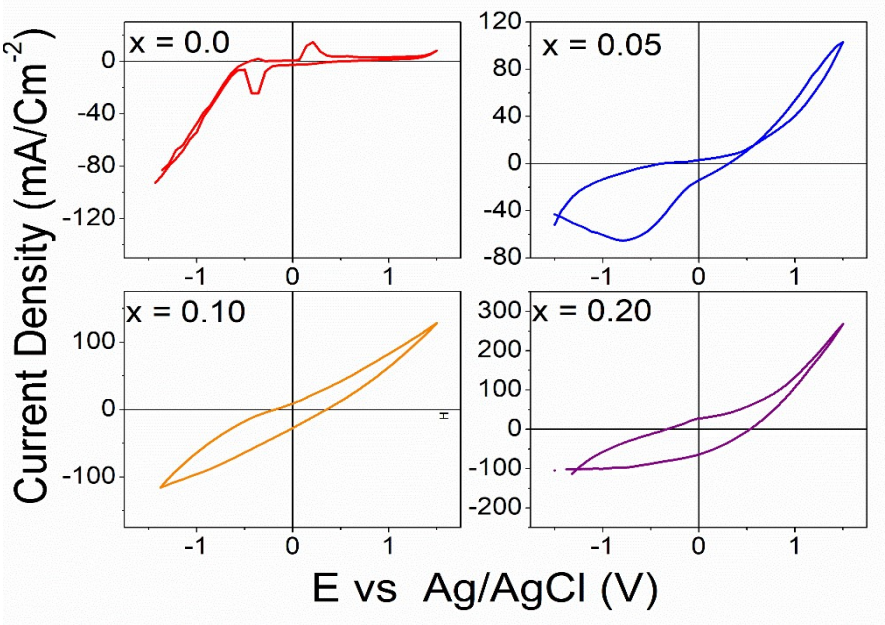

Figure 5.6: Cyclic voltammetry curve for $Pr_{1-x}Ba_{1+x}Co_2O_{6-\delta}$ at 50 mV/s scan rate

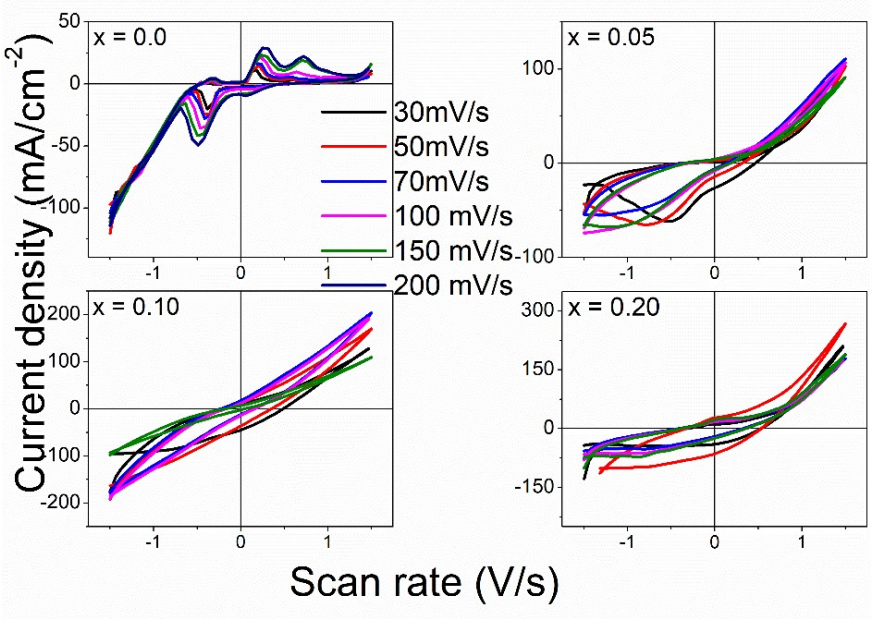

Figure 5.7: Cyclic Voltammetric curves for the $Pr_{1-x}Ba_{1+x}Co_2O_{6-\delta}$ with the different scan rates

The specific capacitance was calculated from the CV curves using the following equation:

$$C = \frac{\int I(v)dv}{mv\nabla V} \qquad (5.3)$$

Where $\int I(v)dv$ Represent the area under the CV curve, m represent the mass of the electrode samples(in gm), v is scan rate (V/s), and ∇V is the potential window[211]. A high value of specific capacitance is observed at 25 mV/s for all the samples (figure 5.8). The value of the specific capacitance decreases as we increase the scan rate. The high value of specific capacitance at a low scan rate is that charges may get enough time to polarize due to more time available, resulting in a high-value capacitance. This effect is also known as the de Levie effect of porous electrodes[212]. The highest value of specific capacitance observed was 235.66 F/g, 598.40 F/g, and 408.37 F/g for x =0.05, x=0.10 and x=0.20, respectively. The high value observed in these electrode samples is due to higher electronic conduction, which arises because of the higher ionic radius of the dopant at the A site[213]. A table of the value of specific capacitance of reported double perovskite samples and obtained in the

Materials	**Cell configuration**	**Electrolyte Molarity (KOH)**	**Specific Capacitance (F g-1)**	**Reference**
$PrBaMn_2O_{6-\delta}$	Three-electrode setup	6 M	1034.8	[206]
La_2CoMnO_6	Three-electrode setup	6 M	109.7	[207]
La_2FeCoO_6	Three-electrode setup	2 M	831.1	[208]
$Ba_2FeCoO_{6-\delta}$	Three-electrode setup	2 M	820	[209]
LaCuMn	Three-electrode setup	0.5 M	600.29	[210]
$Pr_{0.95}Ba_{1.05}Co_2O_{6-\delta}$	Three-electrode setup	1 M	235.66	In This work
$Pr_{0.90}Ba_{1.10}Co_2O_{6-\delta}$	Three-electrode setup	1 M	598.4	In This Work
$Pr_{0.80}Ba_{1.20}Co_2O_{6-\delta}$	Three-electrode setup	1 M	408.37	In This Work

Table 5.2: Comparision of specific capacitance of well known electrodes with the present work

present work is listed in Table 5.2.

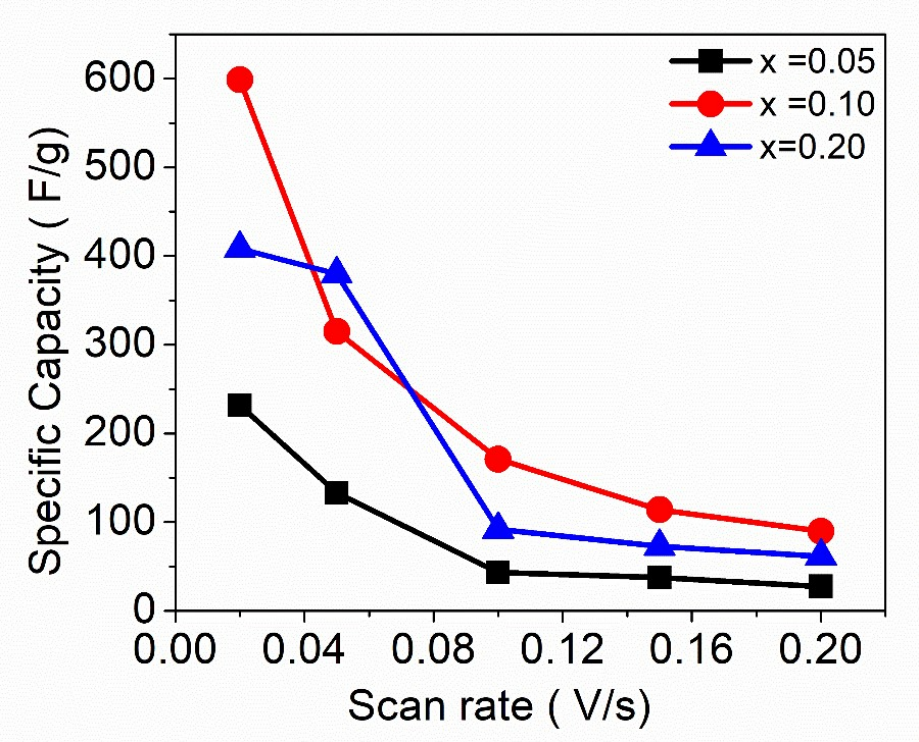

Figure 5.8: Specific capacity of electrodes at various scan rates

In Cyclic voltammetry, the double layer region, where the electrode showing no faradic reaction, general power-law shows the relation between the total current (i) and scan rate (υ) and can be written as [214]:

$$i = a\,\upsilon^{b} \quad (5.4)$$

$$logi = loga + b\,logv \quad (5.5)$$

The b parameter can be calculated from the linear plot of log i and logυ. There is a well-defined parameter for this b value. If the b value is equal to 0.5, then diffusion of oxide ion is dominant in an energy storage mechanism, and the material behaves like a battery. If b equals 1, then the energy storage process is capacitive. For 0.5 < b < 1, there is no explicit limit established, but a region transitional between pseudocapacitive material and battery

type material if b lies in this range [215]. Since the specific capacity of x=0.10 is highest among all synthesized electrodes and seems promising, the relation between log(i) and log(υ) is plotted only for x =0.10 and shown in Figure 5.9(a). The value of b is almost near 0.50 in the range of υ≤100. It confirms that $Pr_{0.90}Ba_{1.10}Co_2O_{6-\delta}$ will behave like a pseudo capacitor. That means the oxide ion diffusion dominates, and the current response should follow the ion diffusion-limited mechanism for electron intercalation or deintercalation[111]. This pseudo capacitance is induced by the intercalation of oxygen ions into the lattice of electrode materials. The mechanism of diffusion-limited oxygen-ion intercalation pseudo capacitance is as follows: Initially, oxygen diffuses from the KOH electrolyte to the surface of active electrode material in the form of hydroxide anion. The oxygen vacancy is then intercalated by the oxygen of the hydroxide anion, which diffuses into the lattice with the oxidation of cobalt. In the meantime, the proton in the electrolyte transfers to the hydroxide anion. The additional oxygen is then intercalated into the perovskite lattice and the surface of the lattice by diffusion of cobalt, present at B site. A slight shift of the positive charge centers of cobalt on the surface toward the oxygen-ions intercalation occurs during this process, providing cobalt a high chemical valence state. The oxygen-ion intercalation was first demonstrated in $LaMnO_3$ in an aqueous KOH solution[216] and has been reported into some other perovskite materials as well[217]–[220]. This diffusion-controlled intercalation process will lead the Randles-Sevcik equation in a specific manner, as mentioned in equation 5.6. According to the equation, the behavior of peak current(i_p) with $\nu^{1/2}$ should be linear. The behavior of the RS equation for x= 0.10 is shown in figure 5.9(b), which is linear, confirming the diffusion-limited mechanism.

$$i_p = 0.45nfAC\left(\frac{nFVD}{RT}\right)^{0.5} \qquad (5.6)$$

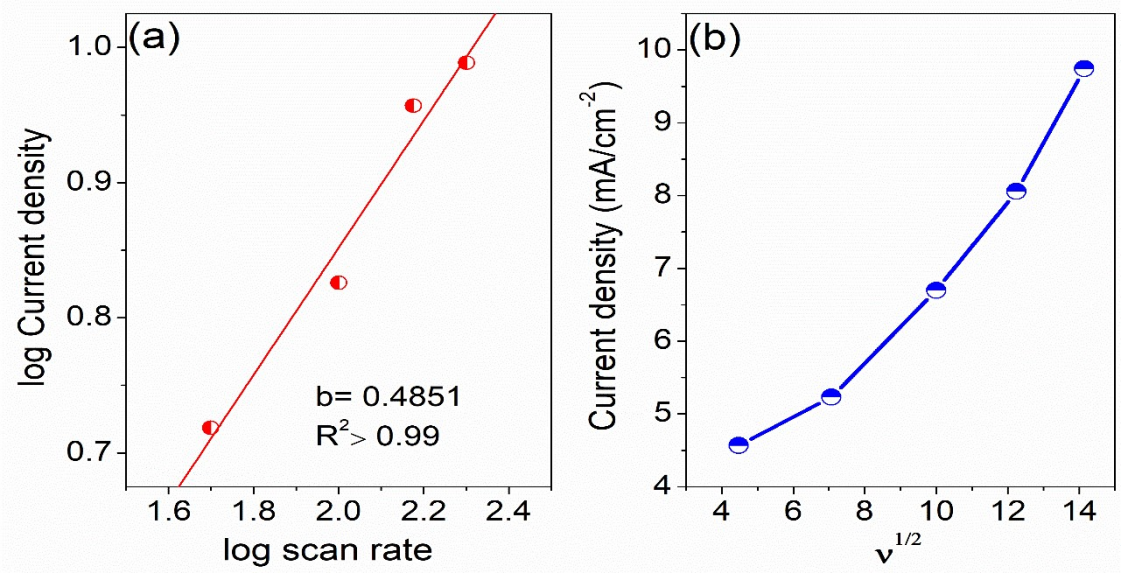

Figure 5.9: (a) The b value corresponding cathodic peak current from CV curves (b) corresponding RS equation for x = 0.10

5.3.5 Catalytic activity for OER

In order to determine the electrochemical performance for OER, electrochemical double-layer capacitance C_{dl} was calculated using cyclic voltammetry data. CV was plotted in a suitable potential range with a scan rate from 20-250 mV/s. In CV curves, the dependency of current density measured across the electrochemical interface on the scan rate can be written as $I = C_{dl}.\frac{dE}{dt}$, where $\frac{dE}{dt}$ is scan rate (ν).[214] However, this study can be performed when the electrolyte/electrode solution interface shows non-faradic behavior. So, for the capacitance of double layer C_{dl}, the difference between the positive and negative current density at half of the scanning range was recorded, and its half value is plotted against the scan rate. The fitted slope of this leads to the C_{dl}. Since electrode sample, x =0.05 shows the electrochemical reversibility during voltammetry, and the highest capacitance is observed in the x = 0.10, the double-layer capacitance was calculated corresponding to these two samples

only shown in figure 5.10. The value of C_{dl} is much higher in the case of x = 0.10 (39.84 mF/cm^2) as compared to x = 0.05 (8.30 mF/cm^2). Electrochemically active surface area (EASA) can be assessed using the obtained value of electrochemical double-layer capacitance C_{dl}. The electrochemically active surface area (EASA) represents the area of the electrode material that is accessible to the electrolyte for charge storage or charge transfer. EASA was estimated according to this equation: $EASA=C_{dl}/Cs$, where Cs represent the specific capacitance of standard electrode materials on a unit surface area[221]. The high value of C_{dl} reveals that the relative electrochemically active surface area of x =0.10 is almost five times x =0.05. This supports the fact that x= 0.10 is more suitable for OER catalyst as compared to the x = 0.05.

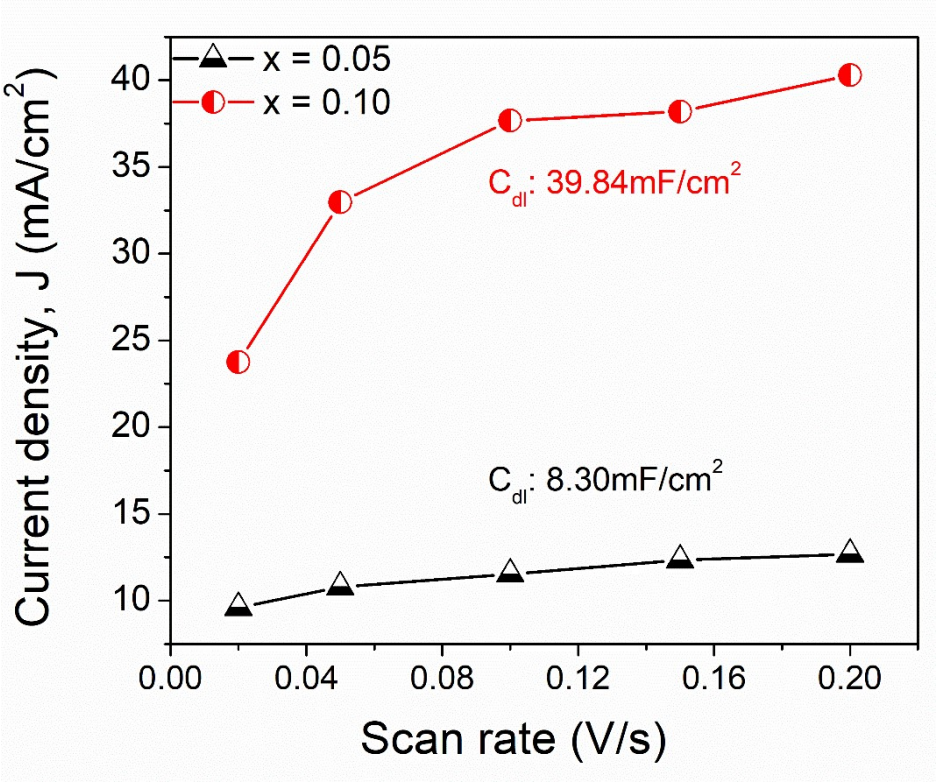

Figure 5.10: Double layer capacitive current density vs. scan rates for the $Pr_{1-x}Ba_{1+x}Co_2O_{6-\delta}$

Another factor that needs to be checked for electrochemical performance is the durability of the Electrode. We carried out the chronopotentiometry measurement by maintaining a constant current density of 10 mA/cm^2 for 10^4 seconds in all electrode samples to check this crucial property. The behavior of all the samples is shown in figure 5.11. All the electrodes offer stable output potential despite slight fluctuation in the starting. This represents the stability of our Electrocatalyst in an alkaline solution.

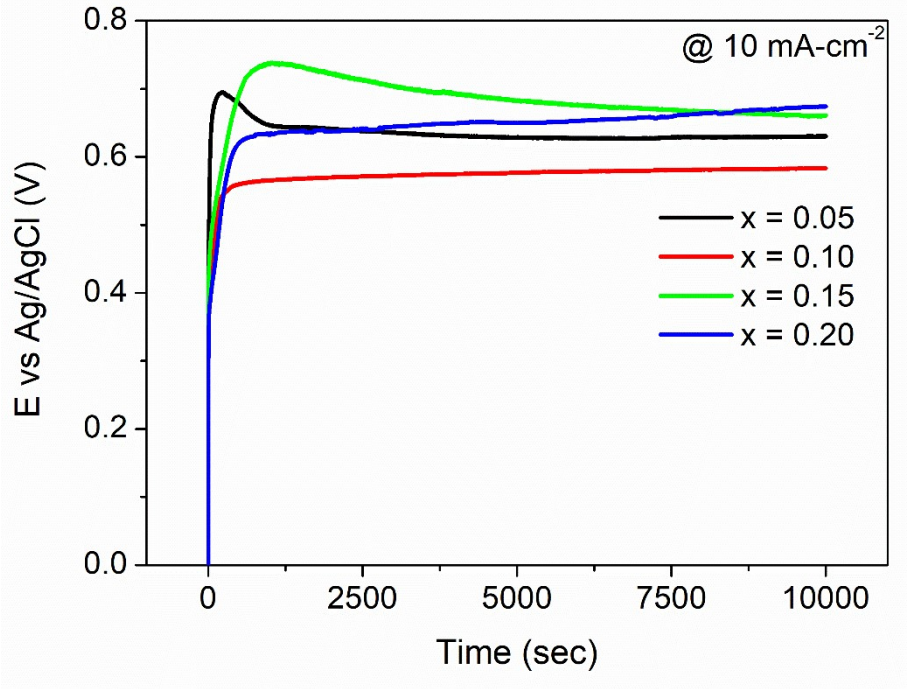

Figure 5.11: chronopotentiometry behavior of all the electrode samples for 10^4 seconds

5.4 Conclusion

In summary, we successfully synthesized a series of double perovskites electrocatalyst $Pr_{1-x}Ba_{1+x}Co_2O_{6-\delta}$ for the first time using the broadly applicable solid-state synthesis method. XRD and Rietveld refinement confirm the phase formation in all electrode samples except for $Pr_{0.85}Ba_{1.15}Co_2O_{6-\delta}$, and SEM images illustrate the electrocatalyst morphology. The detailed electrochemical investigations revealed that x = 0.05 ($Pr_{0.95}Ba_{1.05}Co_2O_{6-\delta}$) exhibits

good ORR activity and a strong redox peak corresponding to the high value of cathodic current with the presence of multiple oxidation states of Cobalt. The specific capacitance for $Pr_{0.95}Ba_{1.05}Co_2O_{6-\delta}$, $Pr_{0.90}Ba_{1.10}Co_2O_{6-\delta,}$ and $Pr_{0.80}Ba_{1.10}Co_2O_{6-\delta}$ (phase pure perovskite) is evaluated to be 235.7, 598.4, and 408.37 F/g, respectively. Power law indicates that oxide ion dominates the energy storage mechanism in $Pr_{0.90}Ba_{1.10}Co_2O_{6-\delta}$, leading to the oxygen-ion intercalation pseudo capacitance, which is corroborated through RS equations. A high value of Double-layer capacitance in $Pr_{0.95}Ba_{1.05}Co_2O_{6-\delta}$ and $Pr_{0.90}Ba_{1.10}Co_2O_{6-\delta}$ reveals the high number of active sites in these two perovskites supporting the high OER activity. However, $Pr_{0.90}Ba_{1.10}Co_2O_{6-\delta}$ is found more suitable for OER catalysts. Since A site substitution of double perovskites praseodymium-based cobaltite is not claimed for the considerable electrocatalyst toward ORR or OER, this study could provide a pathway for efficient and potential application of Pr based double perovskites as an efficient catalyst for OER and ORR.